Journal of Power Sources 188 (2009) 379–386

Contents lists available at ScienceDirect

Journal of Power Sources

journal homepage: www.elsevier.com/locate/jpowsour

Elastic properties of Nafion, polybenzimidazole and poly [2,5-benzimidazole] membranes determined by AFM tip nano-indentation

Esteban A. Franceschini [a], Horacio R. Corti [a,b,*]

[a] Departamento de Física de Materia Condensada, Centro Atómico Constituyentes, Comisión Nacional de Energía Atómica (CNEA), 1650 San Martín, Buenos Aires, Argentina
[b] Instituto de Química Física de los Materiales, Medio Ambiente y Energía (INQUIMAE), Facultad de Ciencias Exactas y Naturales, Universidad de Buenos Aires, Pabellón II, Ciudad Universitaria, 1428 Buenos Aires, Argentina

ARTICLE INFO

Article history:
Received 25 October 2008
Received in revised form 4 December 2008
Accepted 5 December 2008
Available online 11 December 2008

Keywords:
Polybenzimidazole
Nafion
Membranes
Elastic modulus
AFM
Fuel cells

ABSTRACT

The mechanical properties of polybenzimidazole (PBI) and poly [2,5-benzimidazole] (ABPBI) membranes, possible candidates to replace Nafion as proton exchange membranes in direct methanol fuel cells (DMFC), were studied. It was observed by AFM imaging that the morphology of the ABPBI membranes strongly depends on the casting procedure, performed at high temperature from methanesulphonic acid and at low temperature from formic acid. The elastic moduli of the undoped and phosphoric acid doped membranes were determined using the AFM force spectroscopy technique and the differences observed with doped and undoped PBI and Nafion membranes, were discussed in terms of the electrostatic and swelling forces between polymer chains. The analysis of the force curves indicates differences in the mechanical behavior of doped PBI and ABPBI membranes compared to Nafion, which could have practical consequences on the stability of the membrane electrode assemblies.

1. Introduction

Direct methanol PEM fuel cells use Nafion®, a perfluorosulfonated ionomer, as electrolyte membrane [1], or Nafion® composites [2–6]. Due to the dehydration that occurs at temperatures higher than 100 °C and methanol crossover problem associated with the high permeability of methanol through Nafion®, that significantly lowers the electrochemical efficiency of DMPEM fuel cells, several alternative ionomeric materials are being tested, including sulfonated polyarylene sulfones [7,8], polyphosphazene [9], poly [2-2′-(m-fenylene)-5-5′ bibenzimidazole] (PBI, Celazole®) [10], poly [2,5-benzimidazole] (ABPBI) [11], and composite materials of these polymers with inorganic fillers [12–14].

PBI is a neutral commercial polymer (Celazole®) which is a good candidate for DMFC when converted in a Grotthuss proton conductor by acid doping, commonly with H_3PO_4. The properties of PBI membranes relevant to its use in fuel cells have been recently reviewed [15], as well as its high oxidative and thermal stability and low methanol crossover [16,17].

A number of modified PBI polymers were also studied, including sulfonation of the polybenzimidazole [18–20] and the chemical modification of the monomer unit of the polybenzimidazole polymers [11,21,22–25]. One of the simplest polymerization processes to obtain a modified PBI was described by Asensio and Gómez-Romero [22], who synthesized ABPBI, whose chemical structure, along with that of PBI is shown in Fig. 1. We have recently reported the properties of the ABPBI membranes [27], such as phosphoric acid and water uptake, and compare them with PBI and Nafion membranes.

In addition to a suitable ionic conductivity and water/methanol sorption and transport properties, a membrane for DMFC should exhibit good mechanical strength in order to maintain its integrity during the fuel cell assembling and stack construction and to assure durability, especially under high temperature operation. In spite of that, there is a lack of information on the mechanical properties of PBI based membranes.

It is known that pristine PBI has good mechanical properties up to 200 °C [28] and that the sorption of water has a softening effect [29]. Litt et al. [30] found that the acid doping increases the modulus and toughness of PBI-membranes when the number of H_3PO_4 molecules per PBI repeat unit is lower than 2, but the mechanical properties deteriorate dramatically above this doping level. He et al. [31] reported the stress at break of pristine and acid doped PBI membranes as a function of the molecular weight and found that doping levels up to 2.3 have no effect on the stress at break at 125 °C, but decreases by a factor higher than 10 at doping levels

* Corresponding author. Tel.: +54 11 6772 7174; fax: +54 11 6772 7121.
E-mail address: hrcorti@cnea.gov.ar (H.R. Corti).

0378-7753/$ – see front matter © 2009 Elsevier B.V. All rights reserved.
doi:10.1016/j.jpowsour.2008.12.019

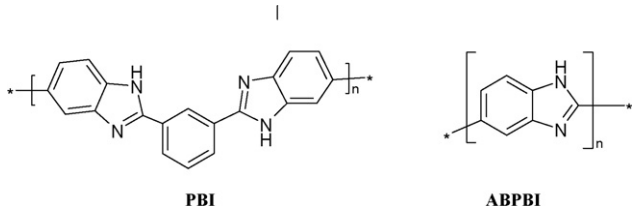

Fig. 1. Structure of PBI and ABPBI.

of 5.6. This behavior was attributed to the deleterious effect of non-bonded acid on the magnitude of the intermolecular forces. Moreover, these authors found that the stress at break increases with the PBI molecular weight.

Xu et al. [32] studied the tensile strength, elongation at break and storage modulus of hyper branched PBI membranes at ambient conditions. The storage modulus of these membranes was comparable to that of linear PBI, but their elongation at break is rather small because of cross-linking.

More recently, Zhang et al. [33] measured the Young's modulus, tensile strength and storage modulus of PBI reinforced with carbon nanofibers (0.5 to 5 wt%). The Young's modulus increases with the nanofibers content, but the tensile strength reaches a maximum around 2 wt% of nanofiber content. The storage modulus for the composites was higher than for the neat PBI and in all cases remains constant up to 300 °C, decreasing sharply above that temperature.

As far as we know, there are not mechanical data reported in the literature for ABPBI membranes. Therefore, the aim of this work is to determine the mechanical properties of ABPBI membranes prepared by high temperature (HT-ABPBI) or low temperature (LT-ABPBI) casting and compares them with PBI and Nafion membranes.

There are several parameters than can be used to describe the mechanical behavior of a polymer [34], but the important one for fuel cell applications is the Young's modulus which account for the stiffness of the material, that is, the resistance of the material to be stretched or compressed. Because the membranes used in DMFC are very thin (few microns) and the interphase mechanical properties of the polymers could be different from the bulk ones, the nano-indentation technique seems to be suitable to analyze these systems in a representative scale [35,36].

On the other hand, there is a particular interest to know the changes in the mechanical properties of these components in different humidity conditions. These interests give place to a wide range of characterizations that are necessary to understand the mechanisms that lead to the optimum behavior of these membranes in the fuel cells.

Here we use the atomic force microscopy (AFM) to measure the local elastic properties of polymeric membranes by force spectroscopy, that is, through the relation between loading force and indentation when the AFM tip indents the membrane surface. The model developed by Stark et al. [37] is used to obtain Young's modulus from the linear part of the force curves. However, exists a big range of experimental data that can be obtained from the slopes of the force curves acquired at different rates. The hysteresis seen in the contact portion of the force curves is related to the viscous properties of the material being indented, as sample friction introduces a phase lag in the cantilever deflection with respect to the scanning position of the piezo scanner [38]. This phase lag increases as the indentation frequency increases. Thus, for a given material, the force curves display larger hysteresis at faster indentation rates, and the rate dependence provides a relative measure of local viscosity of the sample [39].

2. Experimental

2.1. Membrane preparation

The Nafion membrane was a commercial Nafion 117 (Du Pont) with a thickness of around 170 μm.

PBI membranes were prepared from 5 wt% solutions of the commercial powder (Goodfellow) dissolved in N,N-dimethylacetamide (DMA) at 70 °C under stirring. The solution was poured in a glass mold and put in a vacuum furnace at 80 °C during 4 h in order to cast a membrane of thickness ranging from 50 μm to 150 μm. The resulting membrane was immersed in 68.8 wt% H_3PO_4 (10.64 M) at less 72 h prior to use in order to protonate the imidazole ring.

ABPBI was prepared by condensation of 3,4-diaminobenzoic acid (DABA) monomer in polyphosphoric acid (PPA) following the procedure reported by Asensio and Gómez-Romero [22]. The resulting polymer was condensed in water, grinded, and washed with water. Then it was immersed in stirred aqueous 10 wt% NaOH during 20 h in order to eliminate remaining polyphosphoric acid and then washed until neutral pH was attained. Finally it was dried at 90 °C.

High temperature casting ABPBI membranes were made by pouring a 5 wt% solution of ABPBI in pure methanesulphonic on a glass plate kept at about 200 °C over a heating plate inside a ventilated hood. After several hours the solvent was eliminated and the plate was immersed in water to separate the membrane.

Low temperature casting ABPBI membranes were prepared by pouring a 1 wt% solution in formic acid on a Teflon mold and the solvent was evaporated overnight in a ventilated hood at room temperature. Then, the membrane could be easily separated from the mold. All the ABPBI membranes were doped in 10.64 M H_3PO_4 for 72 h to protonate the imidazole ring.

Thick membranes prepared with these casting procedures were used to take standard AFM images and nano-indentation measurements.

In order to diminish the deformation by interaction with the tip during the acquisition of high resolution AFM images, very thin membranes (30–60 nm) were formed over a silicon chip, having a very flat surface, employing diluted solutions (∼1:5000) of the different polymers and using the same casting procedures described above.

2.2. Membrane properties

The molecular weights of polybenzimidazole polymers were obtained by measuring the intrinsic viscosity of their solutions (3, 4 and 5 g dm^{-3}) in concentrated H_2SO_4 (96%). The value of the extrapolated intrinsic viscosity at 30 °C was used to estimate the polymer molecular weight resorting to the Mark–Houwink equation [34] for ABPBI, and Mark–Houwink–Sakurada equation for PBI [31]. The averaged molecular weight of the ABPBI was M_p = 18,800. Even when this molecular weight is lower to that reported by Asensio et al. [11] and by Carollo et al. [21], the degree of polymerization is high enough for casting membranes with good mechanical stability. The molecular weight of PBI, M_p = 19,600, is somewhat lower than that reported by He et al. [31].

The water uptake of PBI and ABPBI doped membranes, determined at 30 °C in the relative humidity range from 0.15 to 1, by using the isopiestic equilibrium method, were reported elsewhere [27]. The water content in doped membranes was expressed by means of λ_w, the number of water molecules per imidazole ring (142 g mol^{-1} for PBI and 116 g mol^{-1} for ABPBI). The sorption isotherms for water have the form of type III in the Brunauer classification, for LT-ABPBI and HT-ABPBI membranes, and are type II-like for PBI membranes. It is also observed that at water activity higher than 0.2 the water uptake by ABPBI membranes is higher than in PBI membranes, and

Table 1
Doping degree (λ_a), at 25 °C and water sorption (λ_w) at 30 °C for PBI and ABPBI membranes doped in 10.64 M aqueous H_3PO_4 [27].

Membrane	M_p (g mol^{-1})	λ_a	λ_w
ABPBI—low T	18,800	3.5	3.35
ABPBI—high T	18,800	2.8	2.19
PBI	19,600	1.9	2.19

LT-ABPBI membranes have higher water uptake than the HT-ABPBI membranes, which is also consistent with the higher acid doping level in the LT-ABPBI membranes. The water sorption of the doped PBI and ABPBI membranes is much higher than the corresponding to Nafion membranes in its protonated form. The water uptake of polymer membranes from vapor phase at the water activity corresponding to 10.64 M aqueous H_3PO_4 is reported in Table 1.

The degree of acid doping, λ_a, the moles of acid per imidazole ring for PBI and ABPBI, are also summarized in Table 1. These results correspond to membranes doped in 10.64 M aqueous H_3PO_4 and in isopiestic equilibrium with the same acid solution at 25 °C ($a_w \approx 0.32$). Only a small fraction of the total up taken acid, about 10%, is not bonded to polymer imidazole groups in the PBI and ABPBI membranes.

2.3. Membrane AFM images

The AFM images of the membranes were acquired using the tapping mode. The AFM parameters to obtain the images were carefully set to minimize the pressure of tip on the membrane fibers, and the silicon surface also could enhance the non-deformability of fibers against the tip pressure [40]. A commercial Si tip having an anisotropic shape was used, with the nominal radius <10 nm, resonant frequency nominal of 300 kHz (315.27 kHz measured), a nominal spring constant of 40 N m^{-1} (36.50 N m^{-1} measured) (MPP-11200 – Veeco Probes – Santa Bárbara, California).

Standard images were obtained over non-supported thick membranes prepared in the conditions that are used in fuel cells Membrane Electrode Assemblies (MEA). On the other hand, high resolution images of the polymer fibers were acquired on thin membranes in order to obtain structural data of the fibers organization in membranes prepared by different casting procedures.

All membranes were stabilized in a nitrogen atmosphere during one hour, to avoid the effect of the adsorbed water over the surfaces.

2.4. Force spectrometry measurement of local elastic properties

A commercial AFM was employed for the measurements (Veeco—DI Multimode Nanoscope IIIa) with 150 μm lateral scan range and a 5 μm z-scanner. The elasticity measurements were done with a Si_3N_4 tip with a spring constant of 0.46 N m^{-1} (Nano Devices, Veeco Metrology, Santa Barbara, California, pyramidal tip shape, cone half angle $a = 18°$, tip curvature radius $r < 10$ nm, resonant frequency nominal: 57 kHz, measured: 47.50 kHz).

For control experiments a stiff mica surface was employed before the measurements to assure the correct operation of the tip, and to verify a suitable spring constant. The set point was 60% of the free oscillation far away from the surface.

As in the case of the AFM images, all measures were carried out in a N_2 atmosphere to avoid the effect of the adsorbed water over the membrane surfaces.

A series of force curves were obtained for each membrane in different positions in order to obtain representative data of the surface. To avoid structural damage of the membranes sample at the point of interest, the tip was first approached carefully to the sample surface and then it was retracted by adjusting the set point to the lowest possible value. Subsequently, the force curve measurements were performed in different points. This procedure was necessary for assessing changes in the shape of the force curves due to sample deterioration induced by the tip. The upper force limit was set to 75 nN and the z-approach speed was 1.74 μm s^{-1} during the force curve acquisition. The sensor response was calibrated on the mica substrate before and after each measurement.

3. Data analysis

The indentation of an AFM tip fixed to a cantilever (spring constant k) into a soft sample (Young's modulus E, Poisson's ratio ν) can be modeled using Hertzian contact mechanics [41]. This theory provides a very simple but direct approach to the material elasticity for a sample with a semi-infinite thickness. For an infinitely hard body indenting (indentation d) into an elastic half space with a normal force F this theory leads to:

$$F = \xi d^m \frac{E}{1-\nu^2} \tag{1}$$

where ξ is a constant dependent on the tip geometry. The exponent m characterizes the indentation behavior. For the indentation of a sphere the exponent is $m = 3/2$ (provided that $d \ll$ sphere radius). A conical indenter with a half angle α leads to $m = 2$.

When the tip exerts a pressure on the sample, the force curve exhibits a given slope, whose value depends on the stiffness of the sample. Considering the indentation $d(z)$, the cantilever deflection, $\delta(z)$, for soft samples becomes,

$$\delta(z) = \begin{cases} -(z - z_0) - d(z), & z < z_0 \\ 0 & z \geq z_o \end{cases} \tag{2}$$

where z_0 is the z piezo position when the tip hits the sample (contact point). The force curves on soft samples can be calculated directly from the Hertz model using Eq. (1). Assuming a cone as a model for the AFM tip, the cantilever deflection *vs.* indentation relation is,

$$d(z) = \left(k\delta(z) \frac{2}{\pi \tan \alpha} \frac{1-\nu^2}{E} \right)^{1/2} \tag{3}$$

where $F(z) = k\delta(z)$ is the loading force, and k is the spring constant. Replacing Eq. (2) for the cantilever deflection in soft samples in Eq. (3), and solving the quadratic equation, the expression for the force curve on an elastic sample is:

$$\delta(z) = \begin{cases} -(z - z_0) \pm \left[\dfrac{a^2}{K^2} - 2\dfrac{a}{K}(z - z_0) \right]^{1/2}, & z < z_0 \\ 0 & z \geq z_0 \end{cases} \tag{4}$$

with $a = (k/\pi \tan \alpha)$, and $K = E/1 - \nu^2$.

It is important to consider that for a very thin sample, the deflection of the cantilever is influenced by the substrate, which restricts the validity of the model. To minimize this problem, sufficiently thick membranes (50–170 μm) were used, so that the influence of the substrate can be neglected.

4. Results and discussion

4.1. High resolution images

In Fig. 2 (a–c), a big difference is observed in the sizes of the membrane fibers depending on the casting method used to prepare them. In the case of LT-ABPBI (Fig. 2a), the fibers are around 25 nm in diameter, while in the HT-ABPBI (Fig. 2b), the polymer fibers seem to form bunches of around 200 nm. This morphology differences could explain not only the different behavior in mechanical properties of the membranes, but also, differences in methanol crossover, water

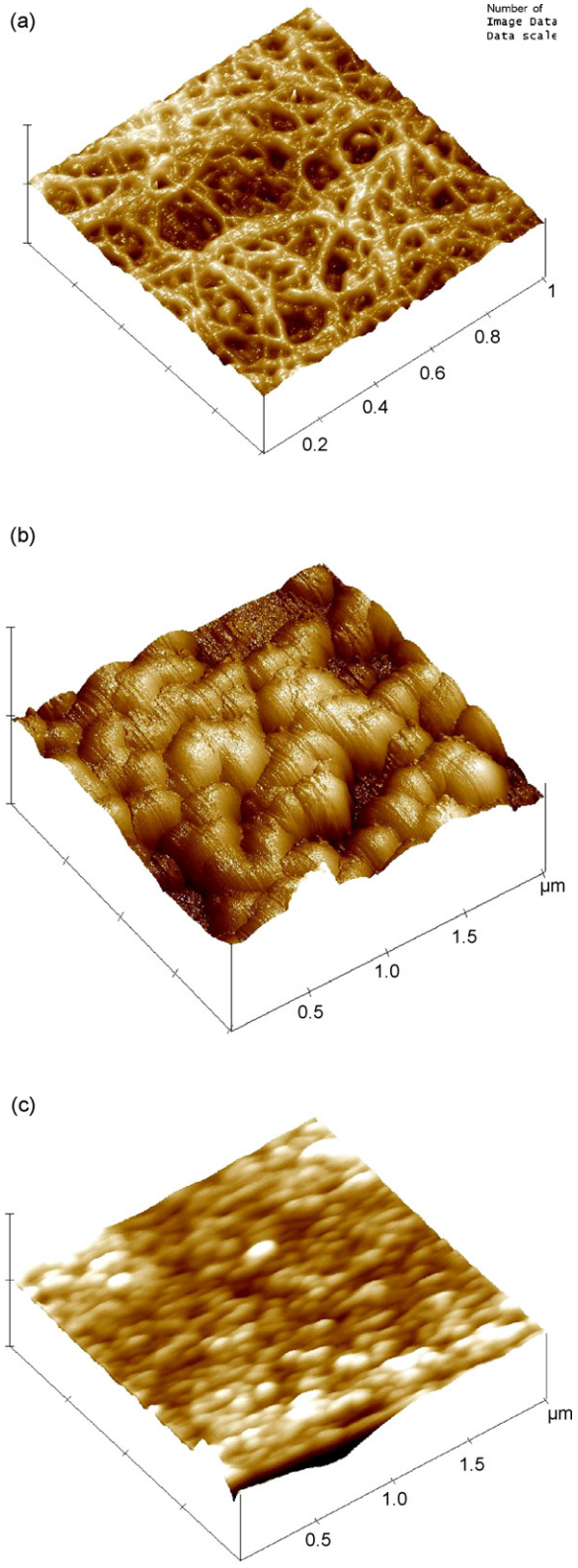

Fig. 2. High resolution 3D AFM images of undoped ABPBI membranes obtained by different casting methods. (a) 1 μm × 1 μm × 0.1 μm image of LT-ABPBI; (b) 2 μm × 2 μm × 0.1 μm image of HT-ABPBI; (c) 2 μm × 2 μm × 0.1 μm image of PBI.

(and H_3PO_4) sorption, proton conductivity, etc., which are fundamental factors for his utilization in fuel cells. Water uptake in ABPBI membranes was measured [27] showing that the LT-ABPBI absorbs more water (and H_3PO_4) than HT-ABPBI. This can be explained considering that larger inter-fiber spaces exist among the smaller fibers in LT-ABPBI as compared to HT-ABPBI, consequently, a bigger number of fibers are exposed to water. In the case of PBI (Fig. 2c), it can be seen that the fibers have a diameter of around 40 nm, and they are much more knotted than in ABPBI, which could originate some of the differences between PBI and ABPBI (LT and HT), with respect to water and acid sorption, Young's modulus, etc.

Table 2
RMS values of the membranes determined on the 10 μm × 10 μm × 2 μm images shown in Fig. 3.

Membrane	RMS (nm)
HT-ABPBI undoped	16 ± 1
HT-ABPBI doped	220 ± 10
LT-ABPBI undoped	50 ± 3
LT-ABPBI doped	68 ± 3
PBI undoped	88 ± 4
PBI doped	12 ± 1
Nafion 117	12 ± 1

4.2. Normal resolution images

Fig. 3 shows the AFM images of doped and undoped HT-ABPBI membrane surfaces, taken in nitrogen atmosphere to avoid water absorption that has deleterious effects on the image quality. The AFM images of doped and undoped PBI and LT-ABPBI membranes, not shown here, exhibit similar characteristics.

It can be seen in Table 2 that all the membranes have similar roughness, measured by the Root Mean Square (RMS), that is, the standard deviation of the Z values within a given area, defined by,

$$\mathrm{RMS} = \sqrt{\frac{\sum_{i=1}^{N}(Z_i - Z_{ave})^2}{N}} \quad (5)$$

where Z_{ave} is the average, Z_i is the current Z value, and N is the number of points within the analyzed area. The RMS mean values and the standard deviations summarized in Table 2 were obtained by analyzing at least 10 images.

It is observed that the acid doping generate changes in the roughness of the membranes, which seems to be strongly dependent on the type of polymer and the casting method employed in their preparation. Thus, the HT-ABPBI presents a dramatic increase in RMS upon doping, much higher than that observed for the LT-ABPBI, while the roughness falls remarkable on doping in the case of the PBI membrane.

It is not clear if the observed behavior could be due to the differences in the conformation of the fibers as revealed in the high resolution images (Fig. 2). However, it is worth to note that among the undoped membranes the highly knotted PBI fibers exhibit the higher RMS. On the other hand, the undoped HT-ABPBI membrane, having the thickest fibers and the lowest RMS, becomes very rough when doped. Unfortunately, high resolution AFM images are very difficult to be acquired for the doped membranes, preventing us of observing conformation changes of the fibers upon doping.

4.3. Young's modulus measurement by force spectrometry analysis

All indentation experiments can be described by the mechanical contact theory (Eq. (4)) and the indentation deeps were shorter than 120 nm. Fig. 4 shows a good agreement with the model of a typical force curve in the approach direction for a Nafion 117 membrane. The value of Young's modulus for Nafion 117 reported in Table 3 was obtained by averaging around 30 curves obtained by indentation in different places of the membrane.

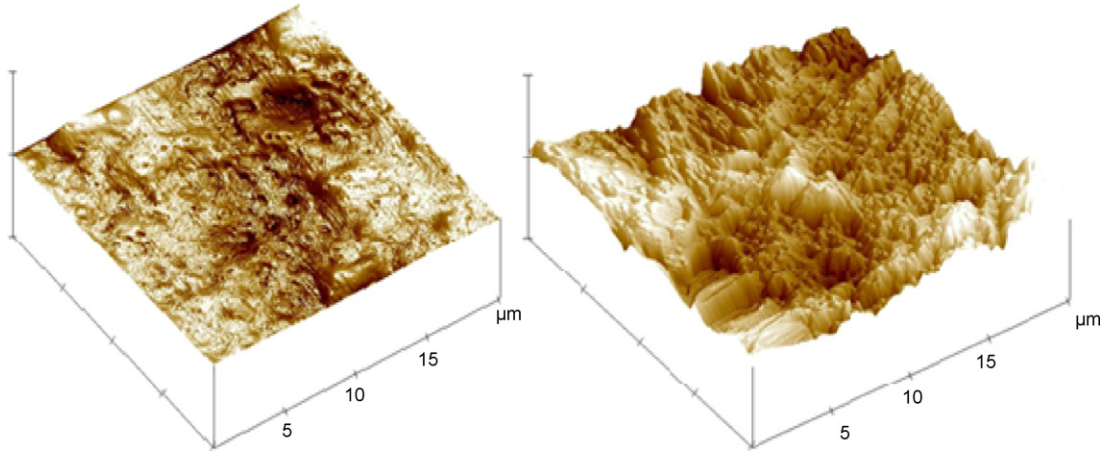

Fig. 3. 3D AFM (20 μm × 20 μm × 2 μm) images of: undoped HT-ABPBI (left); doped HT-ABPBI (right).

Table 3
Young's modulus of the studied membranes.

Membrane	Young's modulus (GPa)
HT-ABPBI undoped	1.19 ± 0.21
HT-ABPBI doped	6.17 ± 0.93
LT-ABPBI undoped	0.290 ± 0.061
LT-ABPBI doped	0.104 ± 0.036
PBI undoped	2.14 ± 0.85
PBI doped	3.60 ± 0.98
Nafion	1.59 ± 0.99

Figs. 5, 6 and 7 show the experimental force curves for PBI, HT-ABPBI and LT-ABPBI membranes, respectively, and the satisfactory fits using the mechanical contact model. In the case of small Young's modulus (undoes and doped LT-ABPBI membranes), the model departures from the experimental values when the indentation exceeds 40 nm. The measured Young's modulus for these membranes, with their respective uncertainties is shown in Table 3. The real uncertainty may be much larger, mainly due to the error in the spring constant of the cantilever.

The Young's modulus decreases when doped with phosphoric acid for LT-ABPBI membranes, but increases for HT-ABPBI and PBI membranes. These results agree with the behavior observed in the laboratory when the casted membranes are manipulated.

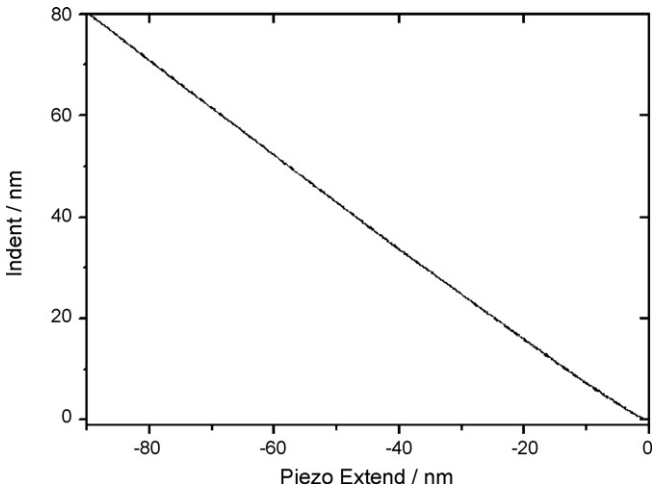

Fig. 4. Indentation curves (solid line) on the Nafion 117 membrane surface. The curve for the model fit (Eq. (5)) matches the experimental one perfectly.

An explanation of these findings could be given in terms of the polymer chain interactions and swelling due to the acid (and water) uptake. The undoped PBI and ABPBI polymer chains are neutral and their interactions are mainly due to hydrogen bond and van der Waals interactions. Once these membranes

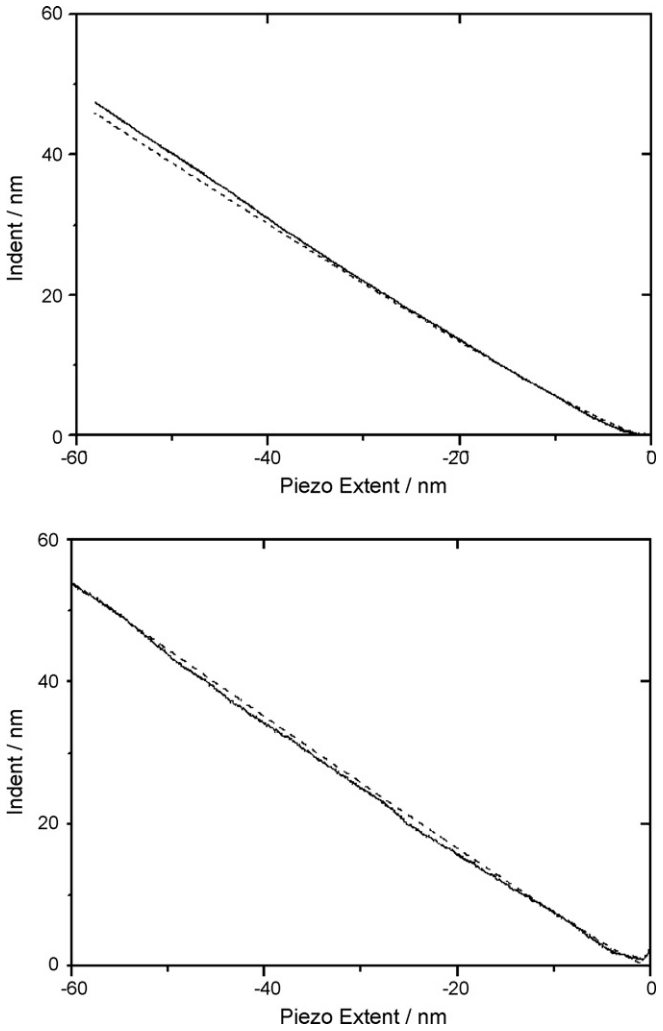

Fig. 5. Indentation curves for undoped PBI (top) and doped PBI (bottom). The solid line corresponds to the experimental data and the dashed line corresponds to the model fit.

are doped with acid, they become protonated and the phosphate anions act as bridges between the chains, creating strong electrostatic interactions. The presence of water, or excess of H_3PO_4, increases the chain separation and decreases the interaction, in such a way that the elasticity of the membranes depends upon a balance between the presence of charges and the water swelling.

The changes observed in the mechanical properties of the membranes when are doped, would depend on the relative magnitude of these effects.

In support of this hypothesis it is important to consider that the LT-ABPBI membranes uptake more water and acid than other membranes, and the predominant effect would be in this case the decreasing of chain interactions due to the high water (or acid) sorption.

It is worth to emphasize that, as far as we know, there are no data in the literature of nano-indentation on this type of membranes, in the conditions that we have studied here. Indeed, other types of mechanical analysis, like tensile stress and mechanical strength [33,42] were reported in different conditions of humidity and/or temperature. Indentation data on Nafion and PBI were only reported in patents and catalogues [43,44] and the experimental conditions were not well defined. In the case of the Nafion, the Young's modulus obtained by nano-indentation of a membrane sample is of approximately 0.7 GPa [43], slightly smaller than that obtained in this work. For PBI, the fabricant reported Young's modulus of 6.2 GPa at 23 °C [44], without specifying neither, the method employed in its measurement (stretching, indentation, etc.), the conditions of humidity, nor the molecular weight of the polymer. Thus, a comparison with the result reported in Table 3 is not relevant.

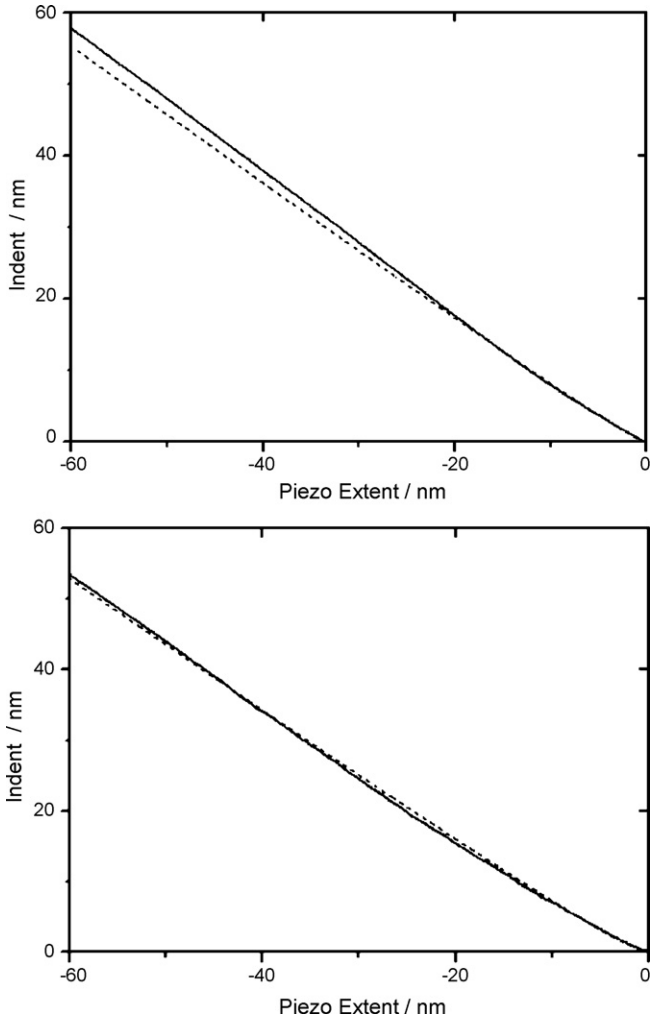

Fig. 6. Indentation curves for undoped HT-ABPBI (top) and doped HT-ABPBI (bottom). The solid line corresponds to the experimental data and the dashed line corresponds to the model fit.

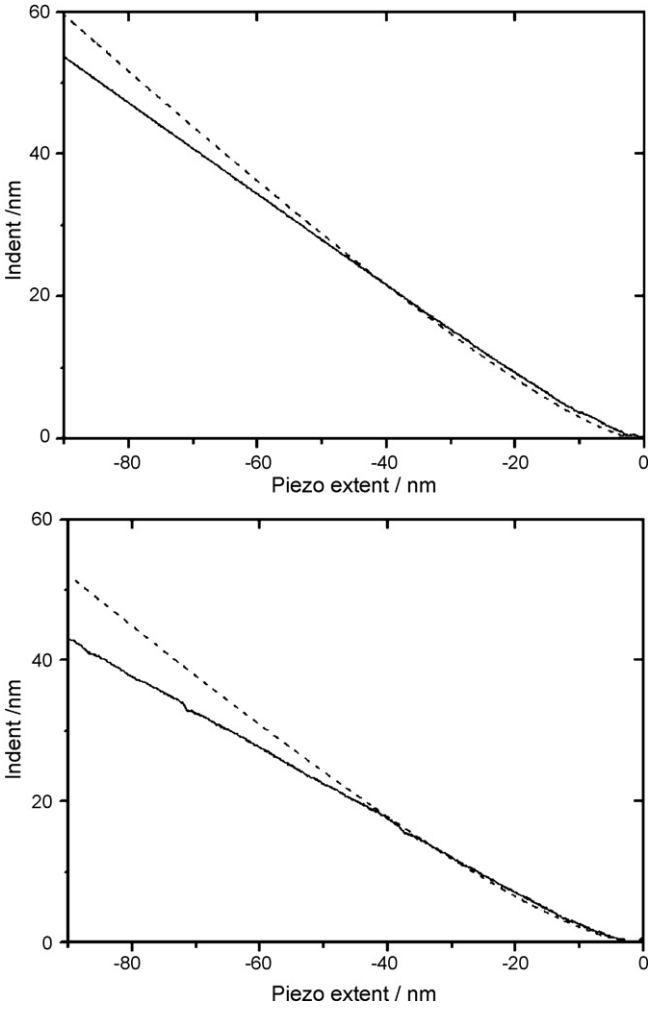

Fig. 7. Indentation curves for undoped LT-ABPBI (top); doped LT-ABPBI (center). The solid line corresponds to the experimental data and the dashed line corresponds to the model fit.

4.4. Force curve analysis

Fig. 8 is a typical force curve for Nafion 117, where the piezo extension data (indentation) and the piezo retraction data are shown. It can be noted that during the indentation does appear neither, signals of a structural breakdown of the sample, nor inelastic deformations, as revealed by the common slopes in the extension and retraction curves. These facts indicate that the samples have an elastic response to the interaction with the tip.

Nevertheless, it is important to consider that, for the Nafion 117 sample, a series of structural breakdowns are observed from $z = 5$ nm up to $z = 110$ nm in the retraction curve. This could be due to the fact that fibers of Nafion are being dragged by the tip when the piezo is retracted. This behavior, not observed in membranes of the PBI, LT- and HT-ABPBI, should be considered in relation to the use of these membranes in fuel cells because they are exposed to compression and decompression processes during the process

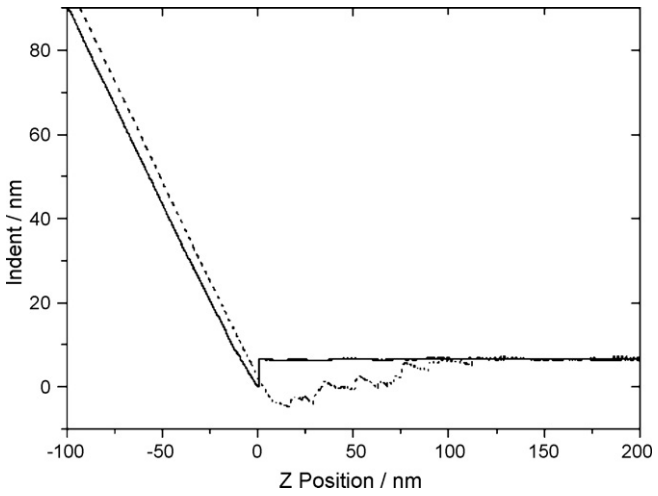

Fig. 8. Force curve for Nafion 117. The piezo extension and retraction data are shown as solid and dashed lines, respectively.

of formation of the membrane electrode assembly (MEA), and a good contact between the catalyst and the membrane needs to be guaranteed.

It can be also seen, (Fig. 9) that when doping the PBI membranes, the fracture region diminish or disappears, indicating an increase in their stability. A similar effect can be seen in ABPBI membranes (HT and LT).

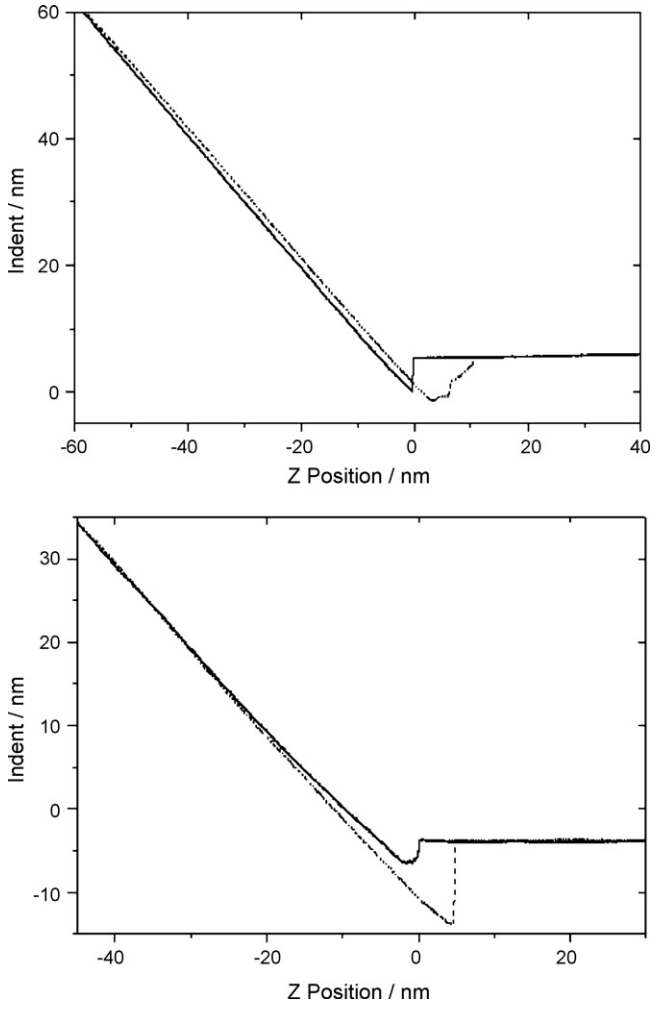

Fig. 9. Force curves for undoped PBI (top) and doped PBI (bottom). The piezo extension and retraction data are shown as solid and dashed lines, respectively.

5. Conclusions

It was probed that the nano-indentation AFM technique could be successfully employed to investigate Young's modulus of fuel cells membranes, such as Nafion, PBI and ABPBI. Our AFM study also included the study of morphological changes of these membranes with the casting and doping methods.

The differences in acid and water sorption depending on the casting method, in the case of ABPBI membranes, and the polymer type (ABPBI, PBI, and Nafion) could account for the observed differences in the behavior of the Young moduli when the membranes are doped. The analysis of the force curves provide a first approach to the study of the deterioration of the membranes with the compression and decompression process, that is an important property for the MEA's construction and durability. It is concluded that doping has a stabilizing effect on the PBI and ABPBI membranes, whereas in the case of the Nafion the compression/decompression processes would generate a wearing down of the membrane.

This work is a first step of a wide range of AFM mechanical and morphological characterizations we have undertaken in order to optimize the behavior of polymer membranes in PEM fuel cells.

Acknowledgments

The authors acknowledge financial support from ANPCyT (PICT Start Up 35403) and Consejo Nacional de Investigaciones Científicas y Técnicas (PID 5977). HRC is a member of Consejo Nacional de Investigaciones Científicas y Técnicas (CONICET). E. Franceschini thanks ANPCyT and CONICET for a graduate fellowship.

References

[1] M.P. Hogarth, T.R. Ralph, Platinum Metals Rev. 46 (2002) 146–164.
[2] P. Staití, A.S. Aricó, V. Baglio, F. Lufrano, E. Passalacqua, V. Antonucci, Solid State Ionics 145 (2001) 101–107.
[3] A.S. Aricó, V. Baglio, A. Di Blasi, V. Antonucci, Electrochem. Commun. 5 (2003) 862–866.
[4] V. Baglio, A.S. Aricó, A. Di Blasi, V. Antonucci, P.L. Antonucci, S. Licoccia, E. Traversa, S. Serraino Fiory, Electrochim. Acta 50 (2005) 1241–1246.
[5] C. Yang, S. Srinivasan, A.B. Bocarsly, S. Tulyani, J.B. Benziger, J. Membr. Sci. 237 (2004) 145–161.
[6] A.S. Aricó, V. Baglio, A. Di Blasi, E. Modica, P.L. Antonucci, V. Antonucci, J. Power Sources 128 (2004) 113–118.
[7] F. Wang, M. Hickner, Y.S. Kim, T.A. Zawodzinski, J.E. McGrath, J. Membr. Sci. 197 (2002) 231–242.
[8] B. Lafitte, L.E. Karlsson, P. Janasch, Macromol. Rapid Commun. 23 (2002) 896–900.
[9] X. Zhou, J. Weston, E. Chalkova, M.A. Hofmann, C.M. Ambler, H.R. Allcock, S.N. Lvov, Electrochim. Acta 48 (2003) 2173–2180.
[10] J.S. Wainright, J.-T. Wang, D. Weng, R.F. Savinell, M. Litt, J. Electrochem. Soc. 142 (1995) L121–L123.
[11] J.A. Asensio, S. Borrós, P. Gómez-Romero, J. Polym. Sci. Part A: Polym. Chem. 40 (2002) 3703–3710.
[12] A.S. Aricó, V. Baglio, P. Creti, A. Di Blasi, V. Antonucci, J. Brunea, A. Chapotot, A. Bozzi, J. Schoemans, J. Power Sources 123 (2003) 107–115.
[13] G. Alberti, M. Casciola, Annu. Rev. Mater. Res. 33 (2003) 129–154.
[14] M.Y. Jang, Y. Yamazaki, J. Power Sources 139 (2005) 2–8.
[15] Q. Li, R. He, R.W. Berg, H.A. Hjuler, N.J. Bjerrum, Solid State Ionics 168 (2004) 177–185.
[16] S.R. Samms, S. Wasmus, R.F. Savinell, J. Electrochem. Soc. 143 (1996) 1225–1232.
[17] J.-T. Wang, S. Wasmus, R.F. Savinell, J. Electrochem. Soc. 143 (1996) 1233–1239.
[18] M.J. Ariza, D.J. Jones, J. Roziere, Desalination 147 (2002) 183–189.
[19] J.A. Asensio, S. Borrós, P. Gómez-Romero, Electrochim. Acta 49 (2004) 4461–4466.
[20] J. Jouanneau, R. Mercier, L. Gonon, G. Gebel, Macromolecules 40 (2007) 983–990.
[21] A. Carollo, E. Quartarone, C. Tomasi, P. Mustarelli, F. Belloti, A. Magistris, F. Maestroni, M. Parachini, L. Garlaschelli, P.P. Righetti, J. Power Sources 160 (2006) 175–180.
[22] J.A. Asensio, P. Gómez-Romero, Fuel Cells 5 (2005) 336–343.
[23] M.K. Daletou, N. Gourdoupi, J.K. Kallistis, J. Membr. Sci. 252 (2005) 115–122.

[24] L. Xiao, H. Zhang, T. Jana, E. Scanlon, R. Chen, E.W. Choe, L.S. Ramanathan, S. Yu, B.C. Benicewicz, Fuel Cells 5 (2005) 287–295.
[25] H. Pu, Q. Liu, G. Liu, J. Membr. Sci. 241 (2004) 169–175.
[27] L. Diaz, G. Abuin, H.R. Corti, J. Power Sources 188 (2009) 45–50.
[28] A. Buckley, D. Stuetz, G.A. Serad, in: J.I. Kroschwitz (Ed.), Encyclopedia of Polymer Science and Engineering, Wiley, New York, 1987, pp. 572–601.
[29] N.E. Iwamoto, NAWCWPNS TP 8036, Naval Air Warfare Center Weapons Division, AD-A262, 93 (1993) 234.
[30] M. Litt, R. Ameri, Y. Wang, R.F. Savinell, J. Wainwright, Mater. Res. Soc. Symp. Proc. 548 (1999) 313–323.
[31] R. He, Q. Li, A. Bach, J.O. Jensen, N.J. Bjerrum, J. Membr. Sci. 277 (2006) 38–45.
[32] H. Xu, K. Chen, X. Guo, J. Fang, J. Yin, J. Membr. Sci. 288 (2007) 255–260.
[33] L. Zhang, Q.Q. Ni, T. Natsuki, Adv. Mater. Res. 47–50 (2008) 302–305.
[34] L.H. Sperling, Introduction to Physical Polymer Science, John Wiley & Sons, New Cork, 1992, pp. 503–554.
[35] A. Hodzic, Z.H. Stachurski, J.K. Kim, Polymer 41 (2000) 6895–6905.
[36] A. Hodzic, Z.H. Stachurski, J.K. Kim, Polymer 42 (2000) 5701–5710.
[37] R.W. Stark, T. Drobek, M. Weth, J. Fricke, W.M. Heckl, Ultramicroscopy 75 (1998) 161–169.
[38] A.B. Mathur, A.M. Collinsworth, W.M. Reichert, W.E. Kraus, G.A. Truskey, J. Biomech. 34 (2001) 1545–1553.
[39] E. A-Hassan, W.F. Heinz, M.D. Antonik, N.P. D'Costa, S. Nageswaran, C.A. Schoenenberger, J.H. Hoh, Biophys. J. 74 (1998) 1564–1578.
[40] D. Alliata, C. Cecconi, C. Nicolini, Rev. Sci. Instrum. 67 (1996) 748–751.
[41] H. Hertz, J. Reine Angew. Math. 92 (1882) 156–171.
[42] H. Kim, E. Cho, J. Han, S.P. Yoon, J. Lee, H.Y. Ha, S. Nam, I. Oh, S. Hong, T. Lim, United States Patent 20,060,211,844 (2006).
[43] Y. Cheng, M.J. Lukitsch, W.R. Rodgers, P.D. Fasulo, United States Patent Application 20,060,068,257 (2006).
[44] Boedeker plastics, Celazole® PolyBenzImidazole Specifications, http://www.boedeker.com/celazo_p.htm.